Properties of magnetotransport in three-dimensional quantum-dot structures

2001 J. Phys.: Condens. Matter 13 1247

(http://iopscience.iop.org/0953-8984/13/6/305)

INSTITUTE OF PHYSICS PUBLISHING JOURNAL OF PHYSICS: CONDENSED MATTER

J. Phys.: Condens. Matter **13** (2001) 1247–1257 www.iop.org/Journals/cm PII: S0953-8984(01)16180-1

Properties of magnetotransport in three-dimensional quantum-dot structures

Weidong Sheng

Beckman Institute for Advanced Science and Technology,
University of Illinois at Urbana-Champaign, Urbana, IL 61801, USA

Received 8 August 2000

Abstract

Magnetotransport through a three-dimensional quantum dot embedded in vertical quantum wires in the presence of parallel magnetic fields is investigated theoretically. The conductance spectra and the electron densities are calculated by the scattering-matrix method. It is found that the characteristics of the magnetoconductance depend strongly on the alignments between the quantum wires and the embedded quantum dot. When the central axes of different components are aligned, the conductance spectra are found to be characterized by antiresonance dips at low magnetic fields and only by plateaus at high magnetic fields. In contrast, when the central axes are misaligned, the conductance spectra are found to be characterized by a mixture of antiresonance dips and tunnelling peaks in the low-magnetic-field region and only by tunnelling peaks in the high-magnetic-field region. A simple but physically motivated model gives an analytical formula which not only compares well with but also provides a reasonable explanation for the numerical data. On the basis of these magnetotransport properties, a method for experimental determination of the alignment of different components in a vertical electronic device is proposed.

1. Introduction

The last few years have witnessed extensive efforts to explore quantum interference effects and ballistic transport in three-dimensional quantum structures. While many researchers studied lateral structures in which the motion of electrons in a two-dimensional system is confined to quasi-one-dimensional movement [1], Reed *et al* [2] studied quantum vertical structures with three-dimensional (3D) confinement and reported evidence of resonant tunnelling through zero-dimensional electron states in an $Al_xGa_{1-x}As/In_yGa_{1-y}As$ column containing a double-barrier structure. Several other experiments [3, 4] on the vertical transport through semiconductor structures have also been reported. In these experiments, the vertical quantum structures were realized either by using a ring-shaped gate around a vertical rod that contains the double-barrier structure in the laterally squeezable region [3] or by using an ion-beam implantation technique to laterally confine a double-barrier quantum well [4]. In addition to these semiconductor

0953-8984/01/061247+11$30.00

structures, vertical ballistic quantum structures were recently realized with metal materials by using scanning tunnelling microscopy [5, 6] and the junction-breaking technique [7], and by atomic force microscopy [8].

A vertical quantum structure often consists of a number of components and its transport properties are largely governed by their configuration. In this paper, we will study how the configuration of different units in a vertical quantum structure affects the magnetotransport properties. We will focus on the vertical quantum wire structure with an embedded quantum dot and show that the system exhibits a clear correlation between the conductance spectra and the alignment between the embedded quantum dot and quantum wires. In particular, the conductances of central-axis-aligned and central-axis-misaligned structures exhibit very distinct characteristics at high magnetic fields: in the perfectly central-axis-aligned structure the conductance recovers its quantization, while in the central-axis-misaligned structure the conductance shows the feature of resonant tunnelling. We shall also discuss, on the basis of the results of this study, an experimental method for the determination of the alignments between different units of a vertical quantum system.

The rest of the paper is organized as follows. In section 2, we describe our model and the method of calculation. In section 3, we present and analyse the calculated conductance spectra and the electron densities for the vertical quantum wire systems with two different alignments. In section 4, we present a one-dimensional model and use it to deduce an analytical formula for the magnetoconductance. In section 5, we discuss possible applications of this study. Section 6 contains a summary and conclusions.

2. The model system and the method of calculation

The quantum systems considered in this work are vertical quantum wire structures, each with an embedded quantum dot, in a longitudinal magnetic field. The quantum wires are assumed to have square cross section and the embedded quantum dot is assumed to be cubic. The Hamiltonian of the system for an electron with a magnetic field applied along the z-axis $\boldsymbol{B} = (0, 0, B)$ is

$$H = \frac{1}{2m^*}(\boldsymbol{P} - e\boldsymbol{A})^2 + U(x, y, z)$$
$$= \frac{1}{2m^*}\left[(P_x + eBy/2)^2 + (P_y - eBx/2)^2 + P_z^2\right] + U(x, y, z) \tag{1}$$

where m^* is the electron effective mass, $U(x, y, z)$ is the potential that defines the lateral electron confinement at z, and $\boldsymbol{A}$ is the vector potential. Here we assume a symmetric gauge for the magnetic field, i.e., $\boldsymbol{A} = (-By/2, Bx/2, 0)$. If the potential U in equation (1) is independent of z, the wave function $\Psi(\boldsymbol{r})$ of the electron at energy E can be expanded in terms of a complete set of lateral modes:

$$\Psi(\boldsymbol{r}) = \sum_{\gamma}\left[a_\gamma e^{ik_\gamma z} + b_\gamma e^{-ik_\gamma z}\right]\Phi_\gamma(x, y) \tag{2}$$

where γ is the index for the lateral modes, k_γ and $\Phi_\gamma(x, y)$ are the longitudinal wavenumber and the wave function for the γth mode, respectively. The lateral modes can be expressed in terms of those for $B = 0$:

$$\Phi_\gamma(x, y) = \sum_{\alpha} F_{\alpha\gamma}\phi_\alpha(x, y) \qquad \alpha = (m, n) \tag{3}$$

$$\phi_\alpha(x, y) = \sqrt{\frac{2}{w_x}}\sin m\pi(x/w_x + 1/2)\sqrt{\frac{2}{w_y}}\sin n\pi(y/w_y + 1/2) \tag{4}$$

where w_x and w_y are the lateral dimensions of the cross section. k_γ and $F_{\alpha\gamma}$ can be obtained by solving an eigenvalue problem (for details, see the appendix).

In a general case where the potential U depends on z, the problem of the magnetotransport of the system may be solved by first dividing the structure along the z-direction into a number of layers, each thin enough to allow us to regard U in it as independent of z, and then using the scattering-matrix (S-matrix) formalism. The S-matrix has a trivial form inside each layer [9]. We will, therefore, in the following, only give the S-matrices for the interface scattering.

Consider two adjacent layers labelled L and R. The S-matrix at the interface between these two layers is defined by

$$\begin{bmatrix} \boldsymbol{B}^{\mathrm{L}} \\ \boldsymbol{A}^{\mathrm{R}} \end{bmatrix} = \mathbf{S}_{\mathrm{I}} \begin{bmatrix} \boldsymbol{A}^{\mathrm{L}} \\ \boldsymbol{B}^{\mathrm{R}} \end{bmatrix} \tag{5}$$

where $\boldsymbol{B}^{\mathrm{L}}$ and $\boldsymbol{A}^{\mathrm{R}}$ are two vectors with elements b_γ^{L} and a_γ^{R}, respectively, while $\boldsymbol{A}^{\mathrm{L}}$ and $\boldsymbol{B}^{\mathrm{R}}$ are two vectors with elements a_γ^{L} and b_γ^{R}, respectively. It is simple to show [9] that the interface S-matrices can be expressed as

$$\mathbf{S}_{\mathrm{I}} = \begin{cases} \begin{bmatrix} -\mathbf{C}\mathbf{F}_{\mathrm{L}} & \mathbf{F}_{\mathrm{R}} \\ \mathbf{F}_{\mathrm{L}}\mathbf{K}_{\mathrm{L}} & \mathbf{C}^{\mathrm{T}}\mathbf{F}_{\mathrm{R}}\mathbf{K}_{\mathrm{R}} \end{bmatrix}^{-1} \begin{bmatrix} \mathbf{C}\mathbf{F}_{\mathrm{L}} & -\mathbf{F}_{\mathrm{R}} \\ \mathbf{F}_{\mathrm{L}}\mathbf{K}_{\mathrm{L}} & \mathbf{C}^{\mathrm{T}}\mathbf{F}_{\mathrm{R}}\mathbf{K}_{\mathrm{R}} \end{bmatrix} & w_{x,y}^{\mathrm{L}} < w_{x,y}^{\mathrm{R}} \\ \begin{bmatrix} -\mathbf{F}_{\mathrm{R}} & \mathbf{C}\mathbf{F}_{\mathrm{L}} \\ \mathbf{C}^{\mathrm{T}}\mathbf{F}_{\mathrm{R}}\mathbf{K}_{\mathrm{R}} & \mathbf{F}_{\mathrm{L}}\mathbf{K}_{\mathrm{L}} \end{bmatrix}^{-1} \begin{bmatrix} \mathbf{F}_{\mathrm{R}} & -\mathbf{C}\mathbf{F}_{\mathrm{L}} \\ \mathbf{C}^{\mathrm{T}}\mathbf{F}_{\mathrm{R}}\mathbf{K}_{\mathrm{R}} & \mathbf{F}_{\mathrm{L}}\mathbf{K}_{\mathrm{L}} \end{bmatrix} & w_{x,y}^{\mathrm{L}} > w_{x,y}^{\mathrm{R}} \end{cases} \tag{6}$$

where $\mathbf{C}$ is a matrix with elements

$$C_{\alpha\beta} = \int\int \phi_\alpha^{\mathrm{L}}(x, y)\phi_\beta^{\mathrm{R}}(x, y)\,\mathrm{d}x\,\mathrm{d}y. \tag{7}$$

Also, $\mathbf{F}$ a matrix with elements $F_{\alpha\gamma}$, and $\mathbf{K}$ a diagonal matrix with elements k_γ.

The overall S-matrix of the entire system can be constructed from all of the individual S-matrices using the composition method [9]. In terms of the overall S-matrix, the conductance in the linear response regime can be expressed as

$$G = \frac{2e^2}{h} \sum_{\gamma,\gamma'} \frac{k_\gamma}{k_{\gamma'}} |(\mathbf{S}_{21})_{\gamma\gamma'}|^2 \tag{8}$$

where γ, γ' are the indices for propagating modes and $\mathbf{S}_{21}$ is the submatrix of the overall S-matrix.

The wave functions, and therefore the electron density, can also be calculated from all the individual S-matrices using the method described in reference [10]. To visualize the electron density we define the particle existence probability $P(\boldsymbol{r})$ from the electron density $\rho(\boldsymbol{r})$:

$$P(\boldsymbol{r}) = \begin{cases} 1 & \rho(\boldsymbol{r}) > \lambda \max\{\rho(\boldsymbol{r})\} \\ 0 & \text{otherwise} \end{cases} \tag{9}$$

where λ is an empirical parameter which is adjusted for the best visual effect. In this paper, we take $\lambda = 0.1$.

3. Magnetoconductance of aligned and misaligned structures

We consider two vertical quantum wire systems as shown schematically in the inset of figure 1 and also that of figure 3—see later. They have different alignments between the quantum wires and the embedded quantum dot. In the following, they are referred to as the central-axis-aligned structure and the central-axis-misaligned structure, respectively. In each of the structures, the quantum wire is assumed to have square cross section, 50 nm × 50 nm, and

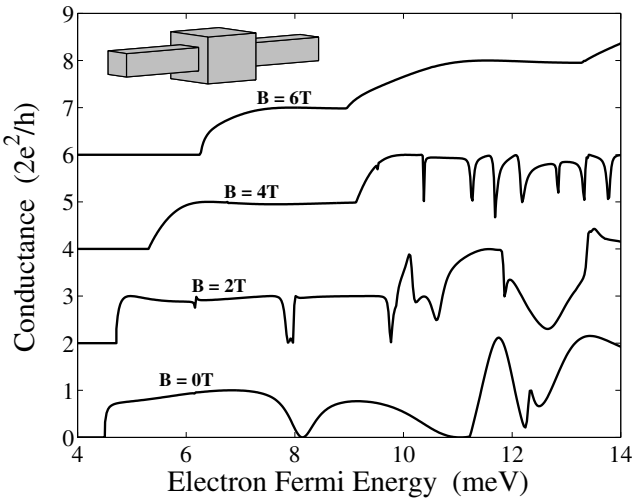

Figure 1. The conductances versus the electron Fermi energy at different magnetic fields for the central-axis-aligned structure shown schematically in the inset. Different curves which are offset vertically for clarity correspond to the marked values of the magnetic field.

the embedded cubic quantum dot to have dimension 100 nm. The effective electron mass is chosen to be $0.067m_e$, which is appropriate for GaAs materials.

Figure 1 shows the calculated conductance of the central-axis-aligned structure as a function of the electron Fermi energy at several different magnetic fields. At zero magnetic field, the conductance spectrum exhibits a smooth structure with broadened dips. We note that the conductance values seen at a Fermi energy larger than 11.2 meV can be higher than the value corresponding to two conductance quanta (i.e., $2 \times 2e^2/h$). This is due to the second and third transverse modes being degenerate in the vertical quantum wires. When a magnetic field is applied, the symmetries of these modes are changed and this degeneracy is lifted. At the same time, the conductance spectra change dramatically. For instance, we see several antiresonances on the first conductance plateau at $B = 2$ T, while at $B = 4$ T a number of sharp resonance dips appear on the second conductance plateau but a rather perfect conductance quantization is found on the first plateau. At $B = 6$ T, all of the sharp resonance dips seen on the first plateau at $B = 2$ T and on the second plateau at $B = 4$ T have disappeared and the quantization on these plateaus is recovered. A qualitative feature seen here is therefore that the conductance spectrum undergoes a transition from that characterized by antiresonance dips at weak magnetic fields to that characterized by a plateau structure at high magnetic fields.

This feature can be understood with the help of the calculated electron densities. They are shown in figure 2 with the upper panel for $B = 0$ and the lower panel for $B = 6$ T. As the probability distribution would exhibit a strong energy dependence if the energy was in the vicinity of the transmission resonance [10], the electron Fermi energy is chosen to be 7.8 meV, far away from any resonances (the position of the nearest resonance at $B = 0$ is about 8.1 meV). At this energy, the transmission is 0.62 at $B = 0$ and 0.99 at $B = 6$ T. The oscillatory probability distribution in the incident quantum wire, seen at $B = 0$, is due to the interference between the incident wave and the reflected wave which occupy the same mode in the incident section. This interference effect becomes much more obvious when the transmission approaches 0.5 at $B = 0$. It could hardly be seen at $B = 6$ T because there is almost no reflected wave at such high magnetic field.

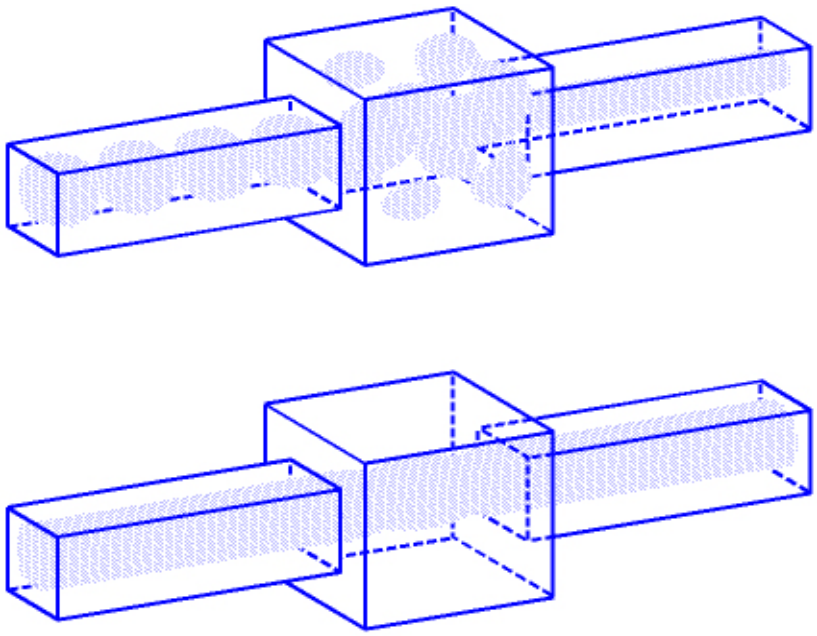

Figure 2. Visualization of the electron density for the central-axis-aligned structure calculated for an electron incident at $E_F = 7.8$ meV. The upper panel is for $B = 0$ T, while the lower panel is for $B = 6$ T. The electron wave is incident from the left lead in both panels.

Let us compare the probability distribution inside the embedded quantum dot at zero magnetic field with that at high magnetic field. At zero magnetic field the probability distribution could be found in most of the quantum dot while it could be seen only along the central axis at high magnetic field. This means that a number of quasibound states [11–13] which have considerable wave amplitudes in the region deviating from the waveguide axis could be coupled to the incident wave at zero magnetic field. However, only those quasibound states which have considerable wave amplitudes at the waveguide axis could be coupled to the incident wave at high magnetic field. As the strong magnetic field compresses the states to the central axes which have perfect alignment for the quantum wires and the quantum dot, the incident wave and the states inside the quantum dot are found to be almost perfectly aligned with each other at high magnetic fields.

It is interesting to note that the conductance spectrum at $B = 4$ T exhibits plateau structure in the first-mode region while it shows a number of antiresonances in the second-mode region (see figure 1). This is because the magnetic field at $B = 4$ T has very different effects on the first two modes in the quantum wires. The first mode is so compressed to the central axis that the electron waves incident in this mode can travel through the embedded quantum dot with little coupling with the quasibound states, which gives rise to nearly perfect transmission. However, this magnetic field is not strong enough to completely suppress the coupling between the second mode and the quasibound states in the quantum dot. As the width of the resonance in energy is determined by the strength of the coupling between the incident mode and the quasibound states, the substantially reduced (not vanishing) coupling would give rise to a number of sharp antiresonances.

The results for the central-axis-misaligned structure are shown in figure 3. It is seen that the central-axis-misaligned structure and the central-axis-aligned structure have very

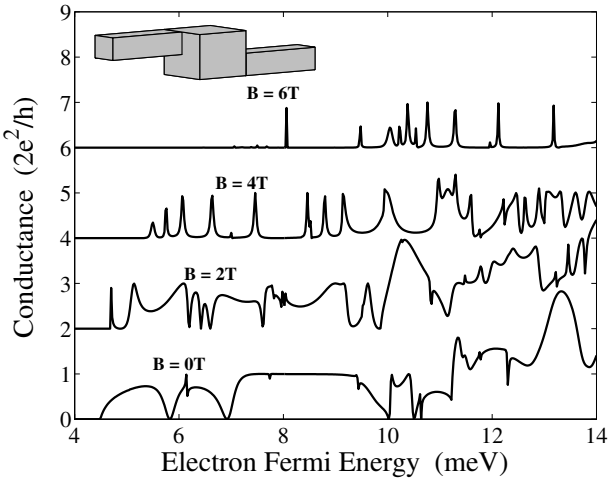

Figure 3. The conductances versus the electron Fermi energy at different magnetic fields for the central-axis-misaligned structure as shown schematically in the inset. Different curves which are offset vertically for clarity correspond to the marked values of the magnetic field.

different conductance characteristics. At zero magnetic field, the conductance of the central-axis-misaligned structure shows more antiresonances. As the magnetic field increases, these antiresonances gradually disappear and resonance peaks emerge. At even higher magnetic fields, the resonance peaks are found to dominate the conductance spectrum. A qualitative feature seen here is therefore that the conductance spectrum of the central-axis-misaligned structure undergoes a transition from that characterized by a mixture of antiresonances and resonance peaks at weak magnetic fields to that characterized by only resonance peaks at high magnetic fields.

In order to understand the characteristics of the magnetoconductance in this structure, we again calculated the electron density at two selected magnetic fields, $B = 0$ and $B = 4$ T. We show the results in figure 4. We choose 6.06 meV as the electron Fermi energy, which is just on the third resonances in the conductance spectrum at $B = 4$ T since this spectrum does not show any feature other than resonance peaks. At $B = 0$, the energy is not on any resonance or antiresonance. As can be seen from the upper panel of figure 4, the incident wave travels through the embedded quantum dot via coupling with several quasibound states. The interference pattern is also obvious in the incident portion where the reflected wave has considerable amplitude. For $B = 4$ T, the lower panel of figure 4 clearly shows a resonant state in the quantum dot.

Although the magnetic field compresses the states to their local symmetry axes in both the central-axis-aligned and the central-axis-misaligned structures, its effects on the conductance spectra of these two structures are very different. As the different portions of the central-axis-aligned structure have a common central axis, the magnetic field enhances the alignment of the electron states in the different portions and, thus, also the possibility of electrons having straight, direct transmission through the quantum dot. However, in the central-axis-misaligned structure, the magnetic field compresses the states in different portions to different central axes and, therefore, suppresses the coupling between the states on either side of the connection interface. Thus, as the magnetic field increases, the direct electron transmission is gradually blocked and the electron transport will be dominated by resonant tunnelling through the localized states in the central quantum dot. This is exactly what we have found in the

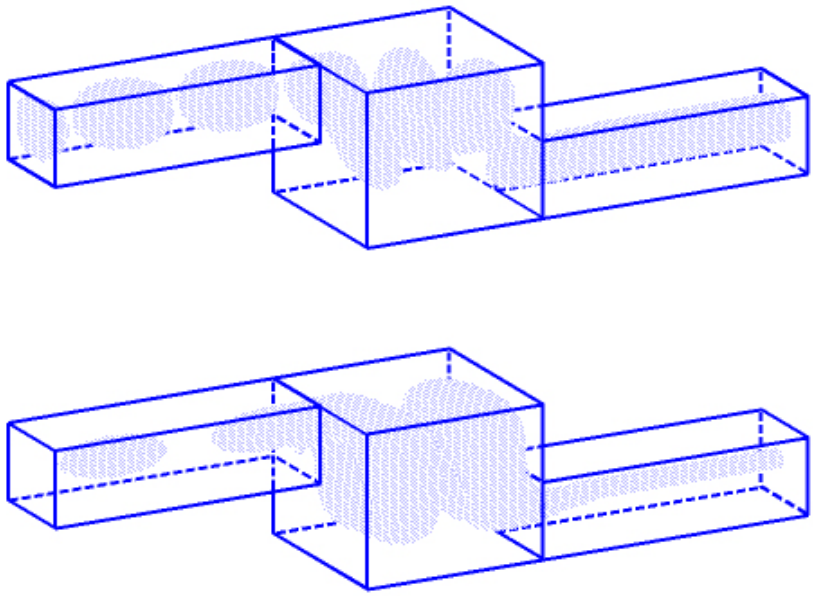

Figure 4. Visualization of the electron density for the central-axis-misaligned structure calculated for an electron incident at $E_F = 6.06$ meV. The upper panel is for $B = 0$ T, while the lower panel is for $B = 4$ T. The electron wave is incident from the left lead in both panels.

calculations as shown in figure 3, where many resonant peaks are seen in the spectra at $B = 4$ T and $B = 6$ T. In the lower panel of figure 4 ($B = 4$ T), the characteristic of a resonant state in the quantum dot can be clearly identified.

4. One-dimensional model

In this section, let us present a one-dimensional model to describe the magnetotransport through the vertical quantum wires. When there is only one propagating mode involved in the transport, it is reasonable to adopt the single-mode approximation [14] if the contribution from the evanescent modes can be neglected. As only one mode is taken into consideration in this approximation, the problem of three-dimensional transport reduces to a one-dimensional one.

Figure 5 shows a schematic view of this model. The central part denotes the quantum dot which is embedded in two vertical quantum wires (denoted by the left and right parts). k and K are the longitudinal wavenumbers of the first transverse modes in the quantum wires and the quantum dot, respectively; c is the coefficient of coupling between these modes, i.e.,

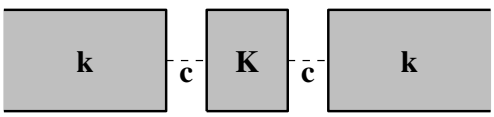

Figure 5. A schematic view of a one-dimensional model. The central part denotes the quantum dot which is embedded in two vertical quantum wires (denoted by the left and right parts). k and K are the longitudinal wavenumbers of the first transverse modes in the quantum wires and the quantum dot, respectively. c is the coefficient of coupling between these modes.

$c = \langle \Phi_1^{\text{wire}} | \Phi_1^{\text{dot}} \rangle$. It is worth noting that the wavenumbers k and K are dependent on both the electron Fermi energy and the magnetic field, while the coupling coefficient c is only dependent on the latter. The total transfer matrix for this model system can be derived as [15]

$$\mathbf{T} = \begin{bmatrix} c & c \\ k & -k \end{bmatrix}^{-1} \begin{bmatrix} 1 & 1 \\ cK & -cK \end{bmatrix} \begin{bmatrix} \mathrm{e}^{-\mathrm{i}KL} & 0 \\ 0 & \mathrm{e}^{\mathrm{i}KL} \end{bmatrix} \begin{bmatrix} 1 & 1 \\ cK & -cK \end{bmatrix}^{-1} \begin{bmatrix} c & c \\ k & -k \end{bmatrix} \tag{10}$$

where L is the length of the quantum dot. The conductance is then given by

$$G = \frac{2e^2}{h} \left| \frac{4c^2 Kk}{(c^2K + k)^2 - \mathrm{e}^{\mathrm{i}2KL}(c^2K - k)^2} \right|^2 . \tag{11}$$

As mentioned in the last section, high magnetic fields would enhance the coupling of the states in the quantum wires and the quantum dot if they were aligned well with each other; otherwise, the coupling would be suppressed. For the central-axis-aligned structure, the coupling coefficient is $c = 0.96$ at $B = 6$ T. The result for the conductance calculated from equation (11) is shown in figure 6 (solid line). Comparison of this result with the numerical data (see figure 1) shows good agreement.

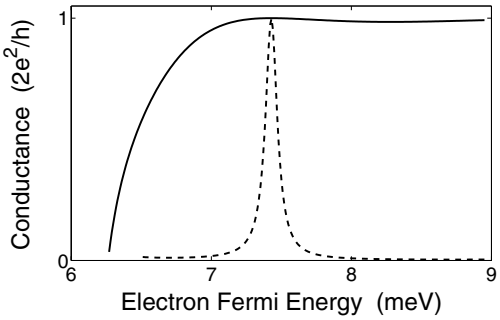

Figure 6. The conductances as functions of electron Fermi energy for two vertical quantum wire structures at $B = 6.06$ T, calculated from the one-dimensional model as described in the text. The solid line and dashed–dotted line respectively correspond to the central-axis-aligned structure and the central-axis-misaligned structure.

For this plateau structure with a smooth transition region, the analytical expression could be further simplified. The transition region starts from the position where the first propagating mode begins to open. In this case, the corresponding longitudinal wavelength is very long, i.e., k is very small and $K \gg k$. This allows us to simplify equation (11) as $G \approx (2e^2/h)4k/[1 - \exp(\mathrm{i}\,2KL)]K$. Considering that

$$\hbar k = \sqrt{E_F - E_1^{\text{wire}}}/2m^*$$

and K changes little in this region, the conductance is expected to behave like a square-root function of the electron Fermi energy in this transition region. This is just what we have found from both figures 1 and 6. When the energy is further increased, the wavenumber k increases and approaches K. Taking $k \approx K$ and $c \approx 1$ into consideration, we could reduce equation (11) to $G \approx (2e^2/h)4Kk/(K + k)^2$ by omitting the term $c^2K - k$ in the denominator. As a result, G will approach $2e^2/h$ when the increased electron Fermi energy suppresses the difference between the two wavenumbers.

For the central-axis-misaligned structure, the coupling coefficient c is only 0.16 at $B = 6$ T. Therefore, the result for the conductance calculated from equation (11), which shows a single resonant peak (see figure 6), is found to be very different from that for the central-axis-aligned

structure. The comparison of this result with the numerical data (see figure 3) shows good agreement, though the resonant peak is found to shift a little. When c is very small, it is elementary to show that the conductance expressed by equation (11) has its peak value ($2e^2/h$) when $\exp(-\mathrm{i}\,2KL) = 1$. The corresponding peak width is proportional to c^2.

5. Discussion

To verify that the magnetic-field-induced transitions are not a characteristic only for the parameters chosen for the numerical calculation, we have checked the results with many other sets of parameters. For structures with larger quantum dots, it is found that the transition occurs at a higher magnetic field for the central-axis-aligned structure while it occurs at a lower magnetic field for the central-axis-misaligned structure. For a central-axis-aligned structure with smooth connections, it is found that the smooth connections have little effect on the conductance characteristics. For a central-axis-misaligned structure, when the length of the smooth connections is 50 nm (the same dimension as that of the quantum wires), the conductance spectra show very similar characteristics to those of the structure with abrupt interfaces. When this length increases to 100 nm, the transitions in the conductance characteristics remain but become somewhat obscured.

Considering the fact that, experimentally, it is more convenient to measure the conductance as a function of magnetic field rather than electron Fermi energy, we show the calculated magnetoconductances for the central-axis-aligned structure (upper panel) and the central-axis-misaligned structure (lower panel) in figure 7. The electron Fermi energy is $E_F = 10$ meV. For other electron Fermi energies, the basic features observed at this Fermi energy remain. From the results, it is clearly seen that the magnetoconductance of systems with different alignments between the quantum wires and the embedded quantum dot exhibit very different behaviours, especially at high magnetic fields. For a system with good alignment between its components, the magnetoconductance shows a transition from that characterized by antiresonance dips at low magnetic fields to that characterized by a smooth structure at high magnetic fields.

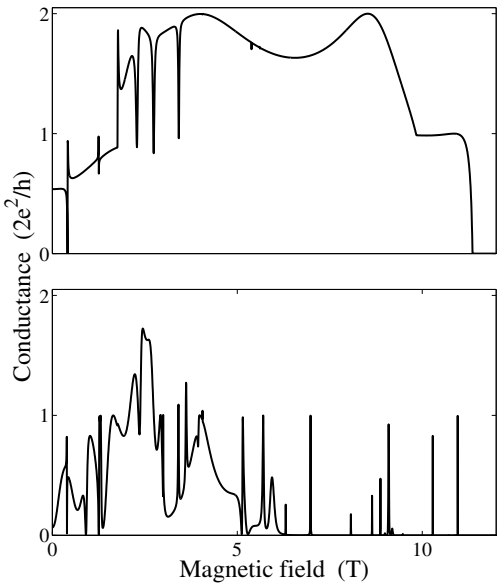

Figure 7. The magnetoconductances for the central-axis-aligned structure as shown in the inset of figure 1 (upper panel) and the central-axis-misaligned structure as shown in the inset of figure 3 (lower panel). The electron Fermi energy is $E_F = 10$ meV.

For a system with misalignment between its components, the magnetoconductance shows a transition from that characterized by a mixture of antiresonance dips and tunnelling peaks in the region of weak magnetic field to that characterized only by tunnelling peaks in the region of high magnetic field. All of these features can be understood in the same way as was described earlier.

Finally, we discuss possible applications of this study. As mentioned in the introduction, electron devices based on nanometre vertical structure are attracting more and more interest. In such devices, the configuration of the different components may be important to the device performance. In many cases, an application requires a good alignment between the different device components [16]. The present study shows that the alignment between different components in a vertical device could be determined by experimental characterization of the magnetoconductances. We should mention that the structures considered in the present study are assumed to be free of any kind of defect. The effect of defects, which is unavoidable in realistic devices, will be investigated in a future study.

6. Conclusions

In this paper, we have studied the magnetotransport in two vertical quantum wire systems with different alignments between the quantum wires and their embedded quantum dots. We have found that the conductance characteristics for the two systems show two different transitions. For the central-axis-aligned system, the conductance spectra are found to be dominated by antiresonance dips in low magnetic fields and only by a plateau structure in high magnetic fields. For the central-axis-misaligned system, the conductance spectra are found to be dominated by a mixture of antiresonance dips and tunnelling peaks in the weak-field region and only by resonant tunnelling peaks in the strong-field region. By using the single-mode approximation, we have obtained the analytical formula for the magnetoconductance, which compares well with and explains the numerical data. Finally, we have proposed that this geometric dependence of the conductance characteristics could be used to determine the alignment of different components in a vertical electron device.

Appendix. Lateral modes in a longitudinal magnetic field

We calculate lateral modes for a vertical quantum wire with a rectangular cross section in a longitudinal magnetic field by solving the following two-dimensional eigenvalue problem:

$$\left\{\frac{1}{2m^*}\left[(P_x + eBy/2)^2 + (P_y - eBx/2)^2\right] + U(x,y)\right\}\Phi_\gamma(x,y) = E_\gamma \Phi_\gamma(x,y). \tag{A.1}$$

On inserting equation (3) into the above equation, this two-dimensional eigenvalue problem reduces to a matrix eigenvalue problem:

$$\sum_{\alpha'} H_{\alpha\alpha'} F_{\alpha'\gamma} = E_\gamma F_{\alpha\gamma} \qquad \alpha = (m,n) \qquad \alpha' = (m',n') \tag{A.2}$$

$$\begin{aligned} H_{\alpha\alpha'} = {} & \delta_{mm'}\delta_{nn'}\frac{\hbar^2\pi^2}{2m^*}\left[\left(\frac{m}{w_x}\right)^2 + \left(\frac{n}{w_y}\right)^2\right] \\ & + \mathrm{i}\frac{2}{\pi^2 m^* w_x w_y} eB\hbar\left[-w_x^2 I_1(n,n')I_2(m,m') + w_y^2 I_1(m,m')I_2(n,n')\right] \\ & + \frac{1}{\pi^3 m^*}\left(\frac{eB}{2}\right)^2\left[w_x^2\delta_{n,n'}I_3(m,m') + w_y^2\delta_{m,m'}I_3(n,n')\right] \end{aligned} \tag{A.3}$$

where

$$I_1(m,m') = \begin{cases} mm'[(-1)^{m+m'}-1]/(m^2-m'^2) & m \neq m' \\ 0 & m = m' \end{cases}$$
$$I_2(m,m') = \begin{cases} 2mm'[(-1)^{m+m'}-1]/(m^2-m'^2)^2 & m \neq m' \\ 0 & m = m' \end{cases} \tag{A.4}$$
$$I_3(m,m') = \begin{cases} 2\pi mm'[(-1)^{m+m'}+1]/(m^2-m'^2)^2 & m \neq m' \\ \pi^3/24 - \pi/4m^2 & m = m'. \end{cases}$$

By solving this matrix eigenvalue problem, we can obtain the eigenvalue E_γ and eigenvector $F_{\alpha\gamma}$ for an electron incident at energy E. The longitudinal wavenumber k_γ is simply given by $\hbar k_\gamma = \sqrt{2m^*(E - E_\gamma)}$.

References

[1] Beenakker C W J and van Houton H 1991 *Solid State Physics: Semiconductor Heterostructures and Nanostructures* ed H Ehrenreich and D Turnbull (New York: Academic) vol 44, p 1 and references cited therein
[2] Reed M A, Randall J N, Aggarwal R J, Matyi R J, Moore T M and Wetsel A E 1988 *Phys. Rev. Lett.* **60** 535
[3] Dellow M W, Beton P H, Langerak C J G M, Foster T J, Main P C, Eaves L, Henini M, Beaumont S P and Wilkinson C D W 1992 *Phys. Rev. Lett.* **68** 1754
[4] Tarucha S, Hirayama Y, Saku T and Kimura T 1990 *Phys. Rev.* B **41** 5459
Tarucha S, Hirayama Y, Saku T and Kimura T 1991 *Phys. Rev.* B **44** 13 815
[5] Olesen L, Laegsgaard E, Stensgaard I, Besenbacher F, Schiøtz J, Stolze P, Jacobsen K W and Nørskov J K 1994 *Phys. Rev. Lett.* **72** 2251
[6] Pascual J I, Méndez J, Gómez-Herrero J, Baró A M, García N and Binh V T 1993 *Phys. Rev. Lett.* **71** 1852
Pascual J I, Méndez J, Gómez-Herrero J, Baró A M, García N, Landman U, Luedtke W D, Bogachek E N and Cheng H-P 1995 *Science* **267** 1793
[7] Krans J M, van Ruitenbeek J M, Fisun V V, Yanson I K and de Jongh L J 1995 *Nature* **375** 767
[8] Junno T, Carlsson S-B, Xu Hongqi, Montelius L and Samuelson L 1998 *Appl. Phys. Lett.* **72** 548
[9] Sheng W D 1997 *J. Phys.: Condens. Matter* **9** 8369
[10] Sheng Weidong and Xu Hongqi 1998 *J. Appl. Phys.* **83** 2146
[11] Tekman E and Bagwell P F 1993 *Phys. Rev.* B **48** 2553
[12] Porod W, Shao Zhi-an and Lent C S 1993 *Phys. Rev.* B **48** 8495
[13] Berthod C, Gagel F and Maschke K 1994 *Phys. Rev.* B **50** 18 299
[14] Wu Hua and Sprung D W L 1993 *Phys. Rev.* B **47** 1500
[15] Sheng W D and Xia J B 1996 *J. Phys.: Condens. Matter* **8** 3635
[16] Wernersson L-E, Litwin A, Samuelson L and Xu H 1997 *IEEE Trans. Electron Devices* **44** 1829